Elastic-Plastic Stress Analysis and Fatigue Lifetime Prediction of Cross-Bores in Autofrettaged Pressure Vessels

Seung-Kee Koh*
Department of Mechanical Engineering, Kunsan National University

Elastic-plastic stress analysis has been performed to evaluate the fatigue life of an autofrettaged pressure vessel containing cross-bores subjected to pulsating internal pressure of 200 MPa. Finite element analyses were used to calculate the residual and operating stress distributions of the pressure vessel due to the autofrettage process and pulsating internal pressure, respectively. Theoretical stress concentration factors of 3.06, 2.58, and 2.64 were obtained at the cross-bore of the pressure vessel due to internal pressure, 50%, and 100% autofrettage loadings, respectively. Local stresses and local strains determined from the elastic-plastic finite element analysis were employed to calculate the failure location and fatigue life of the pressure vessel with radial cross-bores, incorporating the low-cycle fatigue properties of the pressure vessel steel and fatigue damage parameters. Increase in the amount of overstrain by autofrettage process moved the crack initiation location from the inner radius toward a mid-wall, and extended the crack initiation life. Predicted fatigue life of the fully autofrettaged pressure vessel with cross-bores increased about 50%, compared to the unautofrettaged pressure vessel. At the autofrettage level higher than 50%, the failure location and fatigue life of the pressure vessel were not significantly influenced by the autofrettage level.

Key Words : Cross-Bore, Autofrettaged Pressure Vessel, Finite Element Analysis, Fatigue Crack Initiation, Mean Stress, Fatigue Damage

1. Introduction

Largest tensile tangential stress at the inside surface of the pressure vessel subjected to a pulsating high internal pressure causes a fatigue crack initiation and growth from the inside surface. Therefore, to counteract the large tensile tangential stress at the inside surface, autofrettage process which produces compressive tangential residual stresses near the bore of the pressure vessel has been commonly used (Davidson et al., 1963). The autofrettage is a metal forming process by overloading the pressure vessel with high internal pressure, or by passing an oversized mandrel through the bore of the pressure vessel. The compressive tangential residual stresses near the inside surface due to autofrettage process retard crack formation and growth. However, the presence of structural discontinuities which are necessary for engineering purposes of the pressure vessel significantly changes the stress distributions of the pressure vessel and reduces the fatigue life of the pressure vessel due to the stress concentration. For the autofrettaged pressure vessel, the structural discontinuities at the outside surface have been reported as critical locations of early fracture, resulting in shortened fatigue life compared to the unautofrettaged pressure vessel (Koh, 1996; Koh and Na, 1999). It can be ascribed to the high magnitude of tensile tangential stresses and plastic deformation at the discontinuities from the combination of residual stresses by autofrettage, operating stresses by

* **E-mail** : skkoh@ks.kunsan.ac.kr
TEL : +82-63-469-4717 ; **FAX** : +82-63-469-4727
Dempartment of Mechanical Engineering, Kunsan National University, 68 Miryong-dong, Kunsan. Chonbuk 573-701, Korea. (Manuscript **Received** October 7, 1999; **Revised** June 12, 2000)

internal pressure, and stress concentration.

The objective of this study is to analyze the stress and strain distributions of cross-bores in the high pressure vessel subjected to autofrettage loading and cyclic internal pressure of 200 MPa, and thereby evaluate the effects of autofrettage level on the critical location of fatigue cracking and the fatigue life of the pressure vessel. Even though direct comparisons of predicted and measured fatigue lives were not made in this study due to very costly experiments, the fatigue analysis was expected to provide useful information for the design of the autofrettaged pressure vessel under the pulsating high internal pressure.

2. Finite Element Analysis of Cross-Bores in Autofrettaged Pressure Vessels

Fatigue analysis of the autofrettaged pressure vessel with cross-bores subjected to cyclic internal pressure loading requires thorough understanding of the stress distributions. A three-dimensional finite element analysis was performed to find the stress and strain distributions of the autofrettaged pressure vessel with cross-bores. Figure 1 shows the autofrettaged pressure vessel containing ten cross-bores, which penetrate the wall of pressure vessel radially at an angle of 90 degree. In Fig. 1, a, b, and W are inside radius, outside radius, and wall thickness of the pressure vessel, respectively, and d is the diameter of the cross-bore in the pressure vessel. The wall ratio, b/a, of the pressure vessel is 1.53, and the diameter ratio of the cross-bore to the pressure vessel, $d/2a$, is 0.043. Fatigue cracking was expected to occur near the cross-bores due to the stress concentration, and three sources of loadings from the internal pressure of the pressure vessel, autofrettage process, and internal pressure of the cross-bores were considered. The internal pressure on the cross-bores was assumed to be the same as that of the pressure vessel.

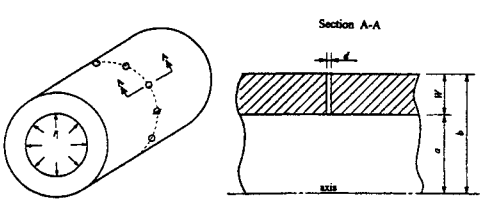

Fig. 1 Configuration of high pressure vessel with radial cross-bores (a=77.5 mm, b=118.2 mm, W=40.7 mm, d=6.65 mm)

In this study, theoretical stress concentration factors of the pressure vessel due to the internal pressure and autofrettage loadings were determined from the linear elastic finite element analysis. An elastic-plastic finite element analysis was also performed to calculate the local stresses and local strains, which were compared to those obtained from an approximate method using the linear elastic stress analysis.

2.1 Elastic stress analysis of cross-bore in autofrettaged pressure vessel

The smooth pressure vessel prior to the introduction of cross-bores was overstrained by autofrettage pressure in order to induce the compressive tangential residual stresses near the inside surface. The tangential residual stresses due to autofrettage are derived as (Hill, 1967),

$$\sigma_\theta=\sigma_{ys}\left\{\frac{a^2}{b^2-a^2}\left(1+\frac{b^2}{r^2}\right)\left[\frac{\rho^2-b^2}{2b^2}-\ln\frac{\rho}{a}\right]+\left[\frac{\rho^2+b^2}{2b^2}-\ln\frac{\rho}{r}\right]\right\},\ \text{for } a\le r\le\rho$$

$$=\sigma_{ys}\left(1+\frac{b^2}{r^2}\right)\left[\frac{\rho^2}{2b^2}+\frac{a^2}{b^2-a^2}\left\{\frac{\rho^2-b^2}{2b^2}-\ln\frac{\rho}{a}\right\}\right],\ \text{for } \rho\le r\le b \tag{1}$$

where σ_{ys} is the yield stress of the pressure vessel steel and r, ρ are radius and elastic-plastic boundary of the autofrettaged pressure vessel, respectively. The stresses due to internal pressure, P_i are given by the following Lame equations (Timoshenko and Gere, 1970).

$$\sigma_\theta=\frac{P_i a^2}{b^2-a^2}\left(1+\frac{b^2}{r^2}\right) \tag{2}$$

Figure 2 shows the finite element model of the pressure vessel containing a cross-bore meshed with three-dimensional eight-noded brick elements. Due to the symmetry of the pressure vessel, only one-twentieth of the total geometry was considered in the finite element model with

Table 1 Linear elastic finite element solutions of maximum tangential stresses and theoretical stress concentration factors at radial hole

Loading type		Max. tangential stress, σ_θ (MPa)			Nominal stress, S_N (MPa)			K_t
		$r=a$	$r=(a+b)/2$	$r=b$	$r=a$	$r=(a+b)/2$	$r=b$	
Pressure (200MPa)		1535.3	1239.6	945.4	501.6	370.9	301.6	3.02
Autofrettage (%O.S.)	50	−779.0	358.2	284.8	−432.8	138.6	112.7	2.58
	100	−908.4	422.2	1122.6	−562.5	33.1	425.2	2.64
Pressure+50%O.S.		-	1594.6	-	-	509.5	-	3.13
Pressure+100%O.S.		-	-	2187.8	-	-	726.8	3.01

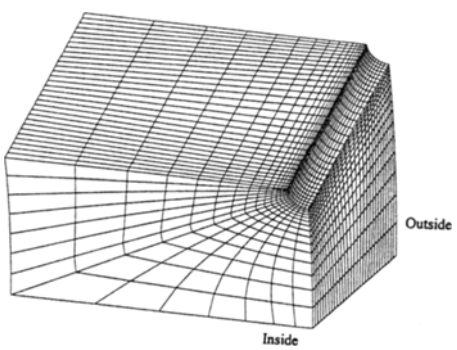

Fig. 2 Finite element model of thick-walled pressure vessel with cross-bores

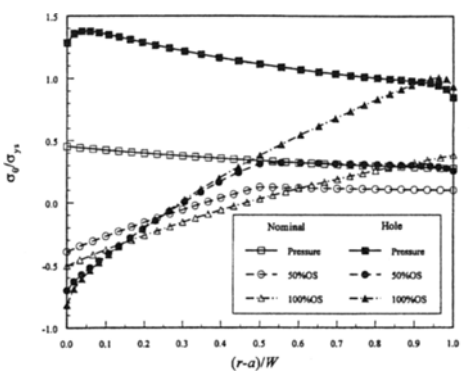

Fig. 3 Nominal and elastic tangential stress Distributions along a cross-bore of pressure vessel for each loading case

appropriate boundary conditions. The mesh was refined until the convergence of the solution was reached. The same internal pressure of 200 MPa was imposed on both surfaces of the pressure vessel and the cross-bore. Plane strain condition was applied by constraining the axial deformation of the pressure vessel, since the open-ended thick-walled pressure vessel was very long. The ANSYS finite element program was employed to perform the thermal and stress analyses (Kohnke, 1992; Koh, 1993).

Nominal tangential stress distributions along the thickness away from the cross-bore are shown in Fig. 3. As the amount of overstrain increased, the magnitude of compressive residual stresses near the inside surface of the pressure vessel increased. The finite element solutions of the tangential stresses along the thickness for each loading case resulted in very close agreement with the theoretical solutions in Eq. (1) and Eq. (2). The differences between finite element and theoretical solutions were less than 2%. Stress concentration due to the introduction of cross-bores increases the magnitude of elastic stresses along the cross-bores, as shown in Fig. 3, depending on the types of loadings. The increasing level of autofrettage amplified not only the magnitude of compressive residual stresses near the inside surface of the pressure vessel, but also the tensile residual stresses at the outside surface, which might be susceptible to fatigue cracking due to high tensile mean stresses in cyclic loading. Therefore, a caution should be required that the autofrettage process rather decrease the fatigue life of the pressure vessel containing structural discontinuities near outside surface.

Theoretical stress concentration factors of the cross-bore at the location where the maximum tangential stress occurs are listed in Table 1. Since the diameter of the cross-bore was relatively small, compared to that of the pressure vessel, the stress concentration factor by the internal pressure was about 3. Tangential stress contours of auto-

frettaged pressure vessel with cross-bore are shown in Fig. 4. The autofrettage residual stresses are compressive at the inside surface and tensile at the outside surface, and the magnitudes of the residual stresses at both inside and outside surfaces increase as the autofrettage level increases, as shown in Fig. 3. Therefore, as the level of autofrettage increases, the location of maximum tangential stress along the cross-bore moved from the inside toward the outside surfaces, resulting from the influence of autofrettage residual stresses.

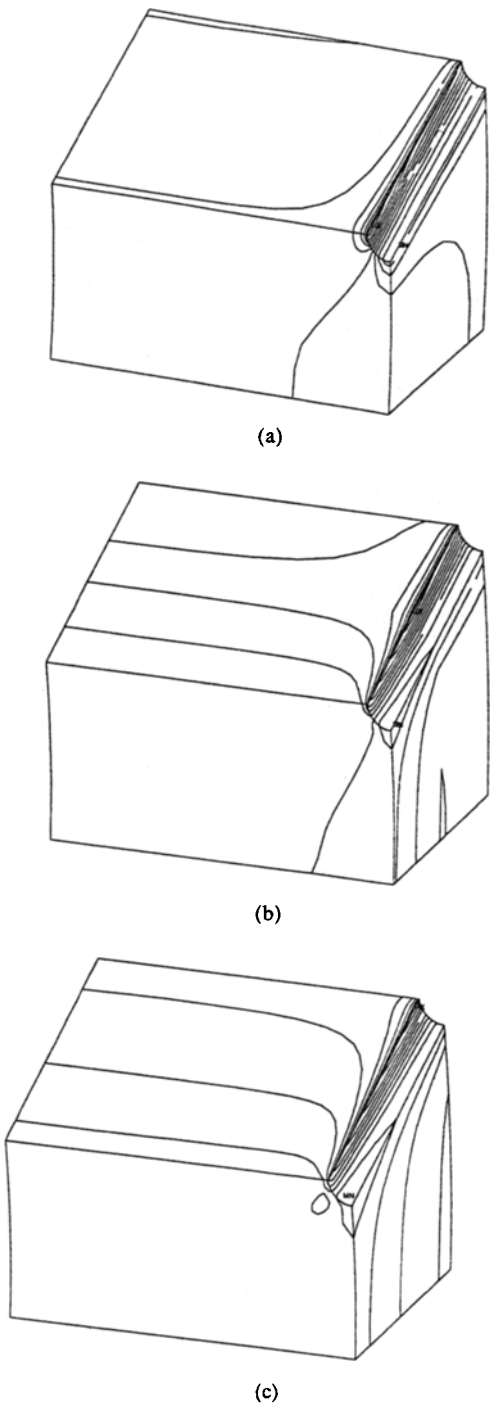

Fig. 4 Elastic tangential stress contours of (a) 0%, (b) 50% and (c) 100% autofrettaged pressure vessels with cross-bores subjected to internal pressure of 200 MPa

2.2 Elastic-plastic stress analysis of cross-bore in autofrettaged pressure vessel

In order to obtain the local deformation of the autofrettaged pressure vessel in the vicinity of cross-bores, an elastic-plastic finite element analysis was performed. Same mesh and boundary conditions used in the elastic analysis were adopted in the elastic-plastic analysis. Kinematic strain hardening rule and von Mises yield criterion were employed in the elastic-plastic finite element analysis. Since the pressure vessel was under cyclic loading, a cyclic stress-strain relation determined from the strain-controlled fatigue testing should be used in the analysis. Monotonic and cyclic properties of the ASTM A723 pressure vessel steel in Table 2 have been obtained in the previous work (Koh et al., 1997), and the cyclic stress-strain curve can be represented as

$$\varepsilon=\frac{\sigma}{E}+\left(\frac{\sigma}{K'}\right)^{1/n'} \tag{3}$$

where σ, ε, n', and K' are cyclic stress, cyclic

Table 2 Monotonic and cyclic properties of cylinder steel

Young's modulus, E (MPa)	197
Ultimate tensile strength, σ_u (MPa)	1264
0.2% offset yield strength, σ_{ys} (MPa)	1112
Elongation, EL (%)	15.5
Reduction in area, RA (%)	46
Fracture strength, σ_f (MPa)	1807
Fracture strain, ε_f	0.617
Hardness, HR_C	43
Cyclic strain hardening exponent, n'	0.083
Cyclic strength coefficient, K' (MPa)	1704
0.2% offset cyclic yield strength, σ_{ys}' (MPa)	1014

strain, cyclic strain hardening exponent, and cyclic strength coefficient, respectively.

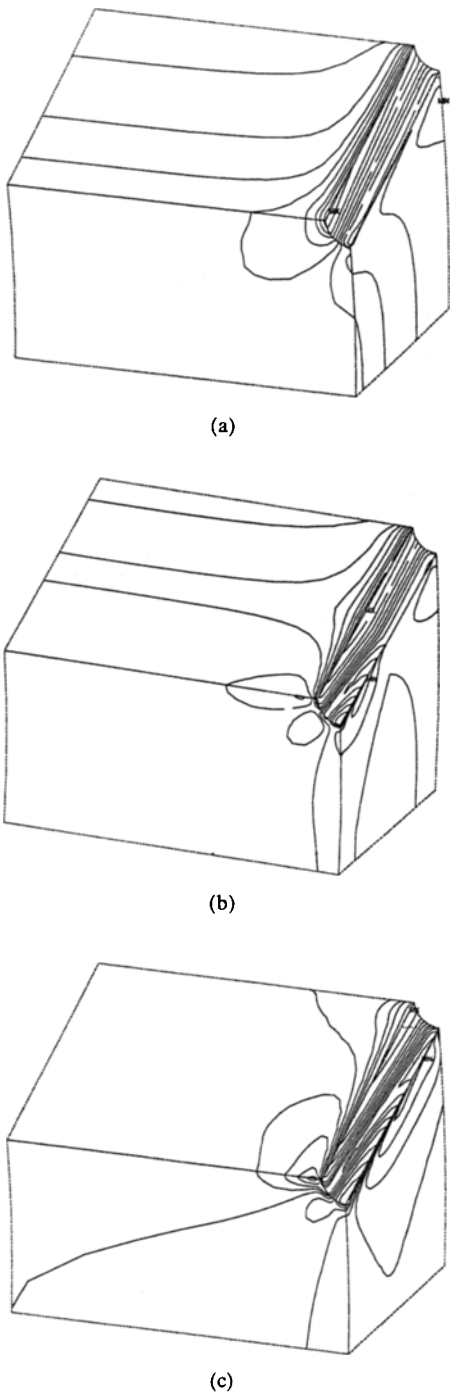

Fig. 5 Equivalent stress contours of (a) 0%, (b) 50% and (c) 100% autofrettaged pressure vessels with cross-bores subjected to internal pressure

Figure 5 shows the equivalent stress contours of the pressure vessel subjected to a combined loading of autofrettage overstrain and internal pressure of 200 MPa. A steep gradient in the vicinity of the cross-bore due to the stress concentration can be observed in Fig. 5. Maximum equivalent stress occurred near the inner wall of the pressure vessel for the unautofrettaged case of 0%OS. However, the location of maximum equivalent stress moved towards the outside wall of the pressure vessel as the amount of overstrain increased. Figure 6 shows the equivalent stress distributions along a cross-bore of the autofrettaged pressure vessel subjected to internal pressure. Four levels of overstrain, i. e., 25%, 50%, 75%, and 100%OS, were considered. From Fig. 6, the autofrettage process considerably decreases the equivalent stress near the inner surface of the pressure vessel, even though the effect seems less pronounced at the high levels of overstrain. A continuous increase in equivalent stress near outside surface of the pressure vessel was observed, as the level of overstrain increased.

Equivalent plastic strain contours for typical % OS are shown in Fig. 7, compared to those for unautofrettaged case. As the %OS increases, the magnitude of the maximum equivalent plastic strain at the cross-bore increases and location of the maximum equivalent plastic strain moves towards the outside surface of the pressure vessel as shown in Fig. 7. It should be noted that the

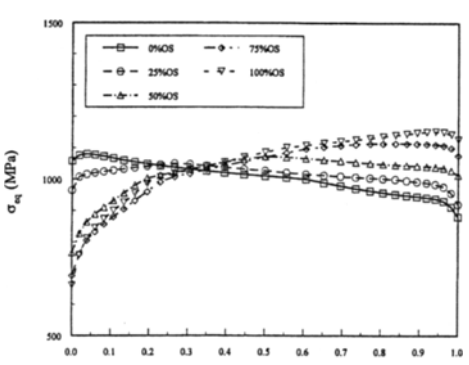

Fig. 6 Equivalent stress distributions along a cross-bore of autofrettaged pressure vessel subjected to internal pressure

magnitudes and distributions of the equivalent stress and plastic strain near the cross-bore depend on the variables such as wall ratio (b/a), diameter ratio (d/a), and autofrettage level (% OS) of the pressure vessel. An elastic-plastic analysis of a pressure vessel with one cross-bore under monotonic internal pressurization by Chaaban and Barake (1993) showed that the amount of plastic deformation near the cross-bore increased, as the diameter ratio and autofrettage level increased and the wall ratio decreased.

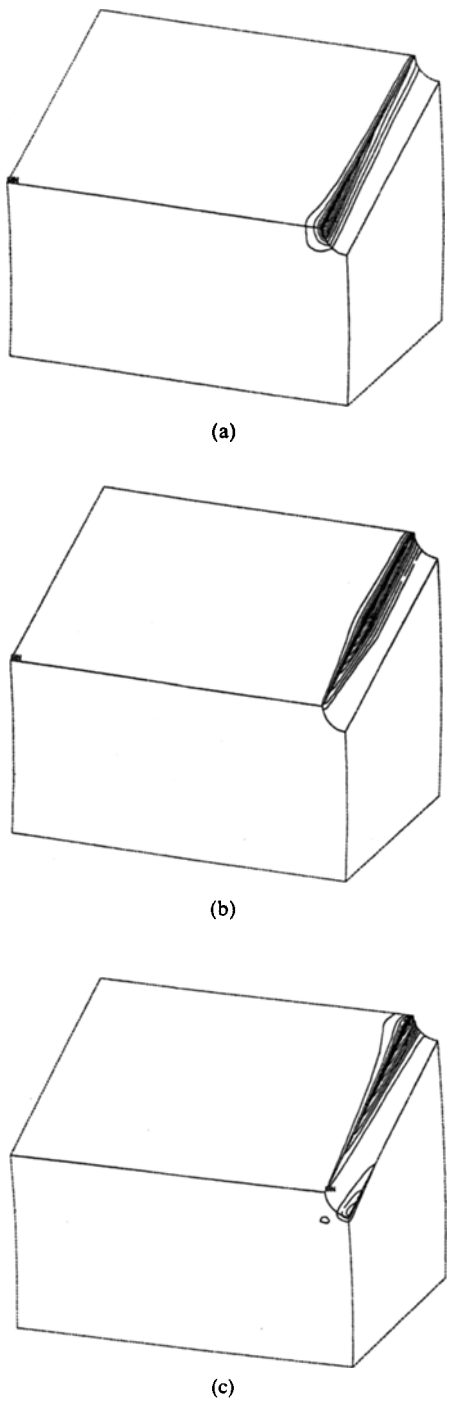

Fig. 7 Equivalent plastic strain contours of (a) 0%, (b) 50% and (c) 100% autofrettaged pressure vessels with cross-bores subjected to internal pressure

The ranges of cyclic stress and strain near the cross-bore in the pressure vessel subjected to the pulsating internal pressure were determined by unloading the internal pressure using a stabilized hysteresis loop curve, which was modeled as twice the cyclic stress-strain curve in Eq. (3). Figure 8 shows the variations of maximum and minimum strains along the cross-bore of the autofrettaged pressure vessel, which is subjected to the cyclic internal pressure loading of 200 MPa. Even though the autofrettage process alleviated the largest tensile stress at the inside surface of the pressure vessel by inducing the compressive residual stress, the strain amplitude due to cyclic internal pressure remained highest at the inside surface. The maximum strain amplitude near the inside surface was 0.0037 with cyclic plasticity, but the cyclic straining for the region of $(r-a)/W \geq 0.2$ was essentially elastic. Strain ratio, $R_\epsilon = \epsilon_{min}/\epsilon_{max}$, along the cross-bore ranged from 0 to 0. 65 for $(r-a)/W \geq 0.2$, resulting in consider-

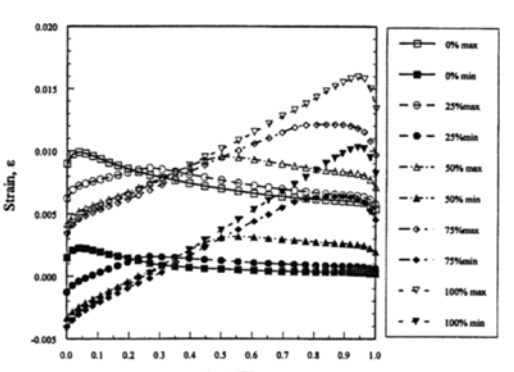

Fig. 8 Variations of strain along a cross-bore of autofrettaged pressure vessel due to pulsating internal pressure

able tensile mean strains and mean stresses during cyclic loading.

3. Fatigue Analysis

3.1 Low-cycle fatigue damage and mean stress parameters

The finite element stress analysis showed that the region along the cross-bore was susceptible to fatigue cracking, ascribed to the stress concentration and high tensile mean stress depending on the level of autofrettage. Fatigue life of the autofrettaged pressure vessel containing cross-bores subjected to pulsating internal pressure can be defined as the sum of the crack initiation life at the critical location and the subsequent crack growth life. In this study, however, the cycles to crack initiation was considered as the fatigue life of the pressure vessel for conservative evaluation.

Fatigue life from the fully reversed strain-controlled test data is mathematically modelled by Basquin and Manson(Fuchs and Stephens, 1980) as,

$$\frac{\Delta\varepsilon}{2}=\frac{\sigma'_f}{E}(2N_f)^b+\varepsilon'_f(2N_f)^c \tag{4}$$

where $\Delta\varepsilon/2$ is the strain amplitude, and σ'_f, ε'_f, b, c are the low-cycle fatigue properties of the ASTM A723 pressure vessel steel as listed in Table 3, determined by using smooth cylindrical uniaxial specimens(Koh, 1996). The low-cycle fatigue damage is known to be significantly influenced by the mean stress. Autofrettage residual stresses play the role of mean stress and thus influence the fatigue life of the pressure vessel. In order to take the mean stress into account, damage parameters from Morrow, Smith-Watson-Topper(SWT), and strain energy density were considered in the fatigue life evaluation.

Morrow equation can be obtained from a modification of the elastic strain-life term in Eq. (4) by introducing the mean stress, σ_m (Graham, 1968).

$$\frac{\Delta\varepsilon}{2}=\frac{\sigma'_f-\sigma_m}{E}(2N_f)^b+\varepsilon'_f(2N_f)^c \tag{5}$$

Table 3 Low-cycle fatigue properties from the fully reversed fatigue test

Fatigue strength coefficient, σ'_f (MPa)	2717.5
Fatigue strength exponent, b	−0.1487
Fatigue ductility coefficient, ε'_f	0.8195
Fatigue ductility exponent, c	−0.9064

A mean stress parameter proposed by Smith et al. (1970) is expressed by the following form.

$$\sigma_{max}\varepsilon_a=C(2N_f)^\gamma \tag{6}$$

where σ_{max} and ε_a are the local stress and local strain amplitude at the critical location such as the cross-bore hole in the autofrettaged pressure vessel, respectively. The coefficient, C and exponent, γ in Eq. (6) for the material were determined as 95.1 MPa and −0.3571 from the fully reversed strain-controlled tests, respectively, and a good correlation with the nonzero mean strain tests was obtained in the previous work(Koh et al., 1997).

The damage parameter using strain energy density, Ψ, can be represented for a uniaxial cyclic loading as(Ellyin and Golos, 1988),

$$\begin{aligned}\Psi&=\Delta W^p+\Delta W^{e+}\\&=\frac{2(1-n')(K')^{-1/n'}}{1+n'}(\Delta\sigma)^{\frac{1+n'}{n'}}+\frac{1}{2E}\sigma^2_{max}\\&=\kappa_u N_f^\alpha+C_u\end{aligned} \tag{7}$$

where ΔW^p is the plastic strain energy per cycle, and ΔW^{e+} is the positive or tensile elastic strain energy per cycle. In the uniaxial cyclic loading, ΔW^p is the area of the hysteresis loop, and $\Delta W^{e+}=\sigma_{max}{}^2/2E$ for $\sigma_{min}\leq 0$ and $\Delta\sigma^2/2E$ for $\sigma_{min}>0$. Mean stress effects are considered in the tensile elastic strain energy term. Material constants, κ_u and α were determined as 550.4 MJ/m^3 and −0.6098, respectively, for the ASTM A723 steel from the fully reversed uniaxial fatigue tests. A material constant, C_u, defined as the energy value corresponding to the fatigue limit of the material, was neglected for the low-cycle fatigue lifetime prediction of the pressure vessel in this study.

3.2 Fatigue life prediction based on elastic stress analysis and Neuber's rule

Fatigue crack initiation life of the pressure vessel was estimated using the local strain approach by incorporating the low-cycle fatigue

Table 4 Local stresses and local strains at a radial hole of autofrettaged pressure vessel determined from Neuber's rule and elastic-plastic finite element analysis

O.S. (%)	Neuber's rule				Elastic-plastic finite element analysis			
	ε_{max}	$\Delta\varepsilon/2$	σ_{max} (MPa)	$\Delta\sigma/2$ (MPa)	ε_{max}	$\Delta\varepsilon/2$	σ_{max} (MPa)	$\Delta\sigma/2$ (MPa)
0	0.01045	0.00381	1096.5	752.1	0.00991	0.00382	1080.6	764.3
50	0.01117	0.00286	1107.9	572.8	0.00956	0.00321	1026.4	642.3
100	0.01952	0.00224	1191.9	447.8	0.01594	0.00283	1152.3	565.6

properties of the material and the finite element stress analysis results. In order to determine the local strains, both approximate and elastic-plastic finite element analyses were used and compared. Fatigue damage parameters accounting for the mean stress effects were considered in the fatigue life prediction. Effects of multiaxial stress state near the cross-bores of the pressure vessel were taken into account by using equivalent stress and strain in the fatigue analysis.

An approximate evaluation of local stresses and local strains at the stress concentrator can be made by using Neuber's rule, stating that the local stress, σ and local strain, ε can be represented in terms of nominal stress, S and nominal strain, e by the following equation (Neuber, 1961).

$$\Delta\sigma\Delta\varepsilon=K_f^2(\Delta S\Delta e) \tag{8}$$

where K_f is the fatigue notch factor, which can be related to the theoretical stress concentration factor, K_t determined from the elastic stress analysis (Peterson, 1980).

$$K_f=1+\frac{K_t-1}{1+\frac{p}{R}} \tag{9}$$

where R is a notch root radius, i. e., cross-bore radius of the pressure vessel, and p is a material property given by $0.0254(2068/\sigma_u)^{1.8}$ mm (Peterson, 1980). Therefore, the maximum local stresses and strains at the cross-bore of the pressure vessel are calculated by solving the cyclic stress-strain relation of Eq. (3), and the Neuber parabola of Eq. (8). It should be noted that a hysteresis loop equation was used to calculate the ranges of local stress and strain in the cyclic loading.

For 0%, 50%, and 100%OS, calculated local stresses and strains using Neuber's rule are listed

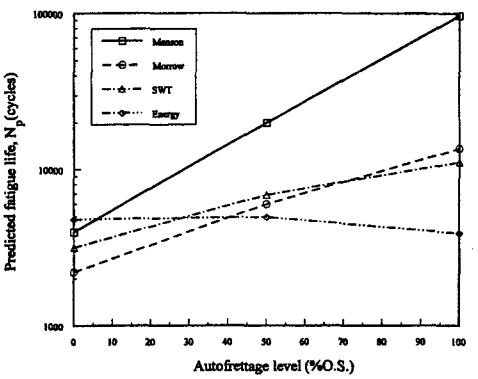

Fig. 9 Predicted fatigue lives of autofrettaged pressure vessels with cross-bores based on Neuber analysis

in Table 4, compared to those obtained directly from the elastic-plastic finite element analysis. The calculated local stresses and strains using Neuber's rule correlated fairly well with the elastic-plastic analysis results. The slight overestimation of the maximum values and underestimation of the amplitudes can be ascribed to the general behavior of Neuber's rule which is based on the plane stress condition.

Neuber's rule is a convenient method of determining the local stress and strain which are used for fatigue life prediction at the critical location. For the autofrettaged pressure vessel, however, the critical location of crack formation was not obvious from the elastic stress analysis, since the maximum values and the amplitudes of cyclic stresses and strains were varying along the cross-bore, as shown in Fig. 3. The elastic finite element stress analysis showed that the location of maximum tangential stress at the cross-bore moved from the inner radius to the outer radius of the pressure vessel as the level of autofrettage in-

creased. Thus, the location of maximum tangential stress at the cross-bore was assumed as the crack initiation region, where the fatigue life was evaluated.

Figure 9 shows the predicted fatigue life of the pressure vessel based on local stresses and strains using the Neuber's rule. In Fig. 9, the fatigue lives predicted by the Manson, Morrow, and SWT parameters increase as the autofrettage level increases. This was attributed to the decrease in strain amplitude at the critical location, which moved toward the outside surface of the pressure vessel, as the autofrettage level increased. However, the fatigue life of the pressure vessel predicted by strain energy density parameter decreased, as the autofrettage level increased. This was mainly due to the relatively large elastic strain energy density at the increased level of autofrettage. Predicted fatigue lives using Morrow, SWT, and energy parameters ranged from 2,208 to 13,624 cycles. Significantly longer fatigue life from Manson equation was evident, since the tensile mean stress, which was detrimental to the fatigue life, was ignored in the life prediction.

3.3 Fatigue life prediction based on elastic-plastic stress analysis

Fatigue damage along the cross-bore of the autofrettaged pressure vessel can be effectively evaluated by using the elastic-plastic finite element analysis. Fatigue damages for various overstrain levels using Morrow, SWT, and strain energy parameters are calculated along the cross-bore as shown in Figs. 10, 11 and 12, respectively. For the unautofrettaged pressure vessel, the largest fatigue damage occurred at the inner radius of the pressure vessel. As the level of autofrettage increased, the location of the largest fatigue damage moved toward the mid-wall of the pressure vessel. It is observed in Figs. 10 and 11 that the fatigue damage calculated by using Morrow and SWT parameters reaches the maximum at r=89.9 mm, i. e., about 0.3W away from the inner surface of the pressure vessel, and the fatigue damage at the critical location is of similar magnitude, regardless of the autofrettage level higher than 50%OS. This implies that the higher level of autofrettage is not always necessary for fatigue life improvement of the pressure vessel, and there may exist an optimum level of autofrettage. When the strain energy parameter is used for the damage evaluation, the location of the highest fatigue damage moves to the outside surface of the pressure vessel as the autofrettage level increases as shown in Fig. 12. This was attributed to the continuous increase in the maximum and mean stresses at the outside surface as the autofrettage level increased, resulting in the increased elastic strain energy density.

In Figs. 10 and 11, the less stiff gradient of the damage curve along the cross-bore for the pressure vessel with autofrettage level higher than 50%OS indicates that a broad cracking region across the thickness may occur due to the evenly

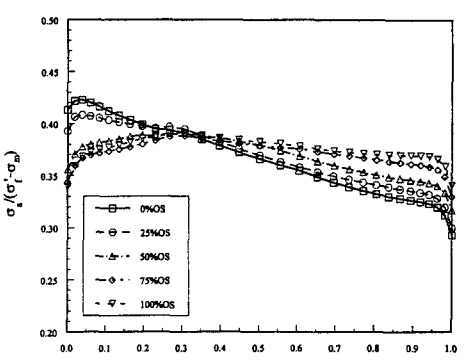

Fig. 10 Damage distributions along a cross-bore of autofrettaged pressure vessls using Morrow parameter

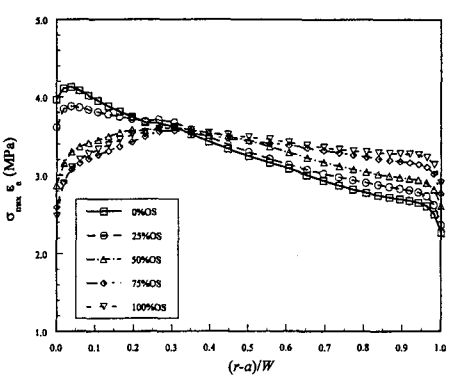

Fig. 11 Damage distributions along a cross-bore of autofrettaged pressure vessls using SWT parameter

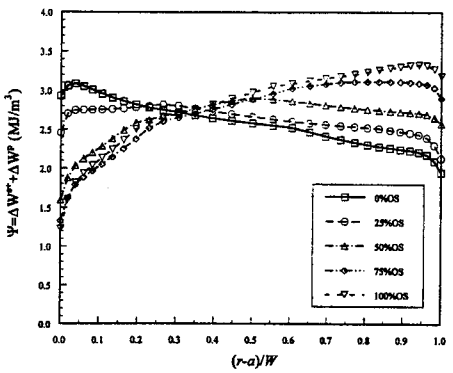

Fig. 12 Damage distributions along a cross-bore of autofrettaged pressure vessls using strain energy parameter

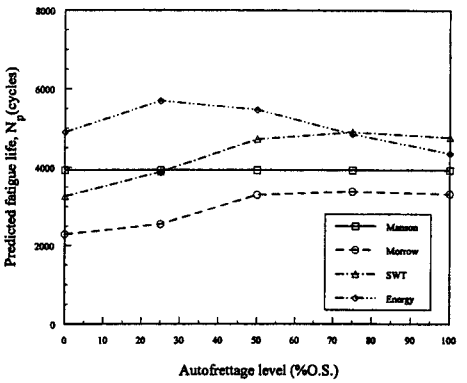

Fig. 13 Predicted fatigue lives of autofrettaged pressure vessels with cross-bores based on elastic-plastic finite element stress analysis

distributed damage, compared to a localized cracking at the inner surface of the unautofrettaged pressure vessel. An autofrettage level of approximately 50%OS seemed to be the optimum for the fatigue life improvement of the pressure vessel with cross-bores subjected to pulsating internal pressure of 200 MPa considered in this study. It should be mentioned that the optimum level of autofrettage may vary, depending on the wall ratio, diameter ratio, magnitude of internal pressure.

Figure 13 shows the predicted fatigue life based on the calculated damage using the elastic-plastic finite element stress analysis. The fatigue life defined as the cycles to crack initiation was evaluated at the critical location of the largest damage along the cross-bore in the pressure vessel. Predicted fatigue life ranges from 2,290 to 4,899 cycles depending on %OS. When the Morrow and SWT damage parameters were used for the life prediction, a 45 percent increase in fatigue life by 50% autofrettage was obtained. At the autofrettage level higher than 50%OS, however, no further improvement was not found. Decrease in fatigue life at the high %OS for the strain energy parameter in Fig. 13 is attributed to the large elastic strain energy component caused by the high residual stresses near the outside surface.

Direct comparison of the predicted fatigue life with the experimentally measured life of the autofrettaged pressure vessel with cross-bores was not possible, since the experiments using the pressure vessel with the same dimensions in the open literature were not available. However, Underwood et al. (1996) measured the fatigue life of the pressure vessel, whose geometry and internal pressure were not the same as the one used in this study. The experimentally observed locations of crack initiation and crack shapes by Underwood et al. were fairly similar to the prediction by using Morrow and SWT damage parameters in this study. Fracture surfaces from the fatigue tests revealed that the fatigue cracking occurred at the localized inside surface for the unautofrettaged pressure vessel and at the broad region along the cross-bore for the fully autofrettaged pressure vessel as predicted in this study. Measured fatigue lives including crack growth of the pressure vessels ranged from 3,500 to 5,000 cycles for 30 to 50%OS level, which were similar to the fatigue lifetime prediction range in this analysis. It was found that the strain energy density parameter overestimated the mean stress effects, thus requiring a modification of the elastic strain energy component for more accurate fatigue life evaluation.

Beneficial influence of autofrettage on the fatigue life improvement of the pressure vessel with cross-bores was not notable, since the favorable compressive residual stress near the inside surface was removed by the cyclic plasticity due to the high stress concentration and the detrimental tensile residual stress near the outside surface of the pressure vessel was produced.

4. Summary and Conclusions

Elastic-plastic stress analysis of cross-bores in autofrettaged pressure vessel subjected to pulsating internal pressure was performed using finite element method. The local stress and local strain obtained from the stress analysis were used for the fatigue lifetime prediction of the autofrettaged pressure vessel with cross-bores and the following conclusions were drawn.

(1) Theoretical stress concentration factors of 3.02, 3.13, and 3.02 were obtained for the pressure vessels subjected to internal pressure of 200 MPa at 0, 50, and 100% autofrettage levels, respectively. As the level of autofrettage increases, the location of maximum tangential stress along the cross-bore moved from the inside to outside surface of the pressure vessel due to the influence of autofrettage residual stresses.

(2) The compressive residual stress due to autofrettage alleviated the largest tensile stress at the inside surface of the pressure vessel. However, the strain amplitude due to cyclic internal pressure remained highest at the inside surface. Cyclic plasticity was observed near the inside surface of the pressure vessel, but the cyclic straining along the cross-bore for the region of $(r-a)/W \geq 0.2$ was essentially elastic with high mean strain and mean stress.

(3) Local stresses and local strains near the cross-bore calculated from Neuber's rule and elastic stress analysis were in fairly good agreement with the elastic-plastic analysis. However, locations of fatigue crack initiation were not obvious from the elastic stress analysis, since the variations of strain amplitude and stress distribution were complex along the cross-bore.

(4) Damage analysis along the cross-bore using elastic-plastic finite element stress analysis indicated that the fatigue cracking location moved from the inner radius to the mid-wall of the pressure vessel as the level of autofrettage increased from 0 to 50%, resulting in extended fatigue life by approximately 50%. However, no significant influence on the fatigue life of the pressure vessel with cross-bores was not observed for the autofrettage level higher than 50%. Predicted fatigue life ranged from 2,290 to 4,899 cycles, exhibiting a similar range to the experimentally measured fatigue life.

Acknowledgements

The author wishes to acknowledge the financial support of the Korea Research Foundation in the year of 1998.

References

Chaaban, A. and Barake, N., 1993, "Elasto-plastic Analysis of High Pressure Vessels with Radial Cross-bores. *High Pressure-Codes, Analysis, and Applications,* ASME PVP-Vol. 263, pp. 67~71.

Davidson, T. E., Kendall, D. P. and Reiner, A. N., 1963, "Residual Stresses in Thick-Walled Cylinders Resulting from Mechanically Induced Overstrain," *Experimental Mechanics,* Vol. 3, No. 11, pp. 253~262.

Ellyin, F. and Golos, K., 1988, "A Total Strain Energy Density Theory for Cumulative Fatigue Damage," *ASME J. Pressure Vessel Technology,* Vol. 110, pp. 36~41.

Fuchs, H.O. and Stephens, R.I., 1980, *Metal Fatigue in Engineering,* Wiley, New York.

Graham, J.A., 1968, *Fatigue Design Handbook,* Society of Automotive Engineers, Warrendale.

Hill, R., 1967, *The Mathematical Theory of Plasticity,* Oxford University Press, Oxford.

Koh, S.K., 1993, "Residual Stress Analysis of an External Grooved Thick-walled Pressure Vessel," *KSME International Journal,* Vol. 7, No. 3, pp. 194~202.

Koh, S.K., 1996, "Fatigue Life Simulation and Estimation of an Autofrettaged Thick-walled Pressure Vessel with an External Groove," *Int. J. Fatigue,* Vol. 18, No. 1, pp. 49~56.

Koh, S.K., Lee, S.I., Chung, S.H. and Lee, K. Y., 1997, "Fatigue Design of an Autofrettaged Thick-walled Pressure Vessel using CAE Technique," *Int. J. Pressure Vessels Piping,* Vol. 1, pp. 19~32.

Lee, S.I., Kim, J.Y., Koh, S.K. and Chung, S.

H., 1998, "Fatigue Crack Propagation Life Evaluation of an Autofrettaged Thick-walled Cylinder," *Transactions of KSME,* Vol. 22, No. 2, pp. 321~329. (In Korean)

Kohnke, P. 1992, *ANSYS User's Manual,* Swanson Analysis Systems, Inc., Houston.

Neuber, H., 1961, "Theory of Stress Concentration for Shear-strained Prismatic Bodies with Arbitrary Nonlinear Stress-strain Law," *J. Applied Mechanics,* Vol. E28, pp. 544~550.

Peterson, R.E., 1980, *Stress Concentration Factors,* John Wiley and Sons, New York.

Smith, K.N., Watson, P. and Topper, T.M., 1970, "A Stress-strain Function for the Fatigue of Materials," *J. Mater.,* Vol. 5, No. 4, pp. 767~778.

Timoshenko, S.P. and Goodier, J.M., 1970, *Theory of Elasticity,* McGraw-Hill, New York.

Underwood, J.H., Parker, A.P., Corrigan, D.J. and Audino, M.J., 1996, "Fatigue Life Measurements and Analysis for Overstrained Tubes with Evacuator Holes," *ASME J. Pressure Vessel Technology* Vol. 118, pp. 424~428.